Characterizing Voltage Losses in an SO_2 Depolarized Electrolyzer Using Sulfonated Polybenzimidazole Membranes

Taylor R. Garrick,[a,b,*,z] Cody H. Wilkins,[a,] Andrew T. Pingitore,[c] Jacob Mehlhoff,[a] Alex Gulledge,[c] Brian C. Benicewicz,[c,*] and John W. Weidner[a,***,z]**

[a]*Hydrogen and Fuel-Cell Center, Department of Chemical Engineering, University of South Carolina, Columbia, South Carolina 29208, USA*
[b]*Electrification Synthesis and Analysis, General Motors Global Product Development, Warren, Michigan 48092, USA*
[c]*Department of Chemistry, University of South Carolina, Columbia, South Carolina 29208, USA*

The hybrid sulfur cycle has been investigated as a means to produce CO_2-free hydrogen efficiently on a large scale through the decomposition of H_2SO_4 to SO_2, O_2, and H_2O, and then electrochemically oxidizing SO_2 back to H_2SO_4 with the cogeneration of H_2. The net effect is the production of hydrogen and oxygen from water. Recently, sulfonated polybenzimidazoles (s-PBI) have been investigated as a replacement for Nafion due to the ability to offer increased process efficiency through the generation of higher acid concentrations at lower potentials. Here, we measure the acid concentrations and individual potential contributions toward the overall operating voltage seen in the SO_2-depolarized-electrolyzer. We then determine model parameters necessary to predict voltage losses in a cell over a wide range of operating temperatures, pressures, currents and reactant flow rates.

Manuscript submitted March 10, 2017; revised manuscript received November 27, 2017. Published December 7, 2017. This was Paper 1141 presented at the San Diego, California, Meeting of the Society, May 29-June 2, 2016.

The hydrogen production program at the U. S. Department of Energy is examining an array of distributed and centralized hydrogen facilities that could contribute to the hydrogen generation infrastructure.[1] Thermochemical cycles are being considered for large scale, centralized facilities due to their potential for high efficiencies at low costs. These cycles involve a series of chemical reactions that result in the splitting of water at much lower temperatures (~500–1000°C) than direct thermal dissociation (>2500°C) and at much higher efficiencies than direct water electrolysis.[2] Chemical species in these reactions are recycled resulting in the consumption of only energy and water to produce hydrogen and oxygen. Although there are hundreds of possible thermochemical cycles, the hybrid-sulfur (HyS) process is the only all-fluid, two step thermochemical cycle.[3–6] The high temperature step (850–950°C) involves the decomposition of H_2SO_4 to produce oxygen and sulfur dioxide via the following reaction:

$$H_2SO_4 \rightarrow SO_2 + \frac{1}{2}O_2 + H_2O \qquad [1]$$

The SO_2 is separated, cooled, and sent to the SO_2-depolarized electrolyzer (SDE). The resulting reactions at the anode and cathode, respectively, are:

$$SO_2 + 2H_2O \rightarrow H_2SO_4 + 2H^+ + 2e^- \qquad U^0_{SO2} = 0.158\ \text{V vs. SHE} \qquad [2]$$

$$2H^+ + 2e^- \rightarrow H_2 \qquad U^0_{H2} = 0\ \text{V vs. SHE} \qquad [3]$$

Thus, the overall reaction in the electrolyzer is represented as:

$$SO_2 + 2H_2O \rightarrow H_2SO_4 + H_2 \qquad [4]$$

Considerable progress was made in the last decade in lowering the operating voltage and increasing the current density of the SDE by moving from a microporous rubber diaphragm separator used by Westinghouse[7] to a perfluorinated sulfonic acid membrane (e.g., DuPont's Nafion).[8–12] For example, Westinghouse was only able to get the cell voltage down to 1.0 V at 400 mA/cm^2, where we achieved 500 mA/cm^2 at 0.71 V and 1.2 A/cm^2 at 1.0 V using Nafion 212 (N212). However, to achieve overall process efficiency, concentrated sulfuric acid as well as low cell voltage at high current densities are necessary. The key issue when using membranes like Nafion that rely on water for their proton conductivity is that high acid concentrations dehydrate the membrane and dramatically increase membrane resistance. In our previous work,[10–12] the water needed for Reaction 2 was controlled by varying the pressure differential across the cell, which in turn affected both the cell voltage and acid concentration.

Figure 1 illustrates the tradeoff between these two performance metrics. When there is no differential pressure ($\Delta P = 0$) across Nafion,

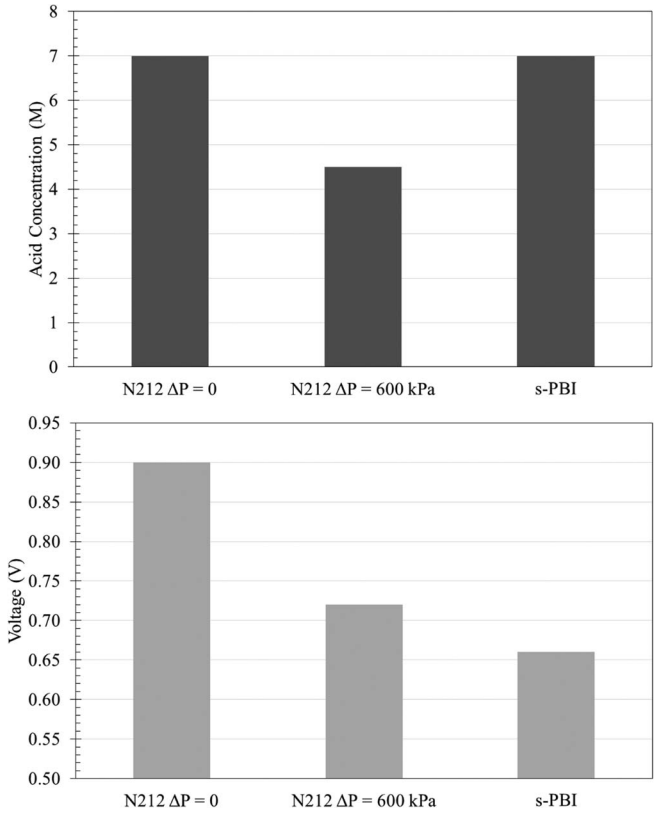

Figure 1. a) Sulfuric acid concentration and b) cell voltage at 0.5 A/cm^2 for: Nafion at 80°C and two pressure differentials (ΔP);[11] and sulfonated polybenzimidazole (s-PBI) at 110°C.

*Electrochemical Society Member.
**Electrochemical Society Student Member.
***Electrochemical Society Fellow.
[z]E-mail: taylor.garrick@gm.com; weidner@cec.sc.edu

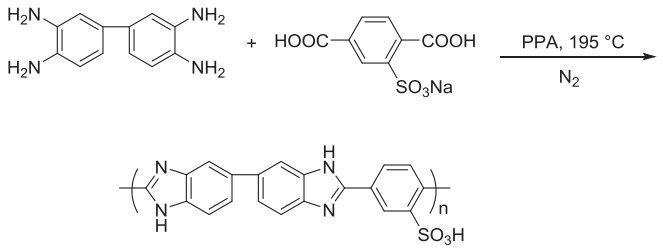

Figure 2. Synthesis of s-PBI using mono-sodium-2-sulfoterephthalate and 3'3',4,4'-tetraaminobiphenyl in polyphosphoric acid (PPA).

minimal water crosses from the cathode to the anode, resulting in high acid concentrations and high cell voltages (7.0 M and 0.90 V at 80°C and 0.5 A/cm^2 respectively). When a differential pressure is created ($\Delta P = 600$ kPa) additional water crosses over the membrane, lowering the cell voltage at 0.5 A/cm^2 from 0.9 V to 0.72 V through an increase in the membrane conductivity. However, this additional water results in a decrease in the acid concentration from 7.0 M to 4.5 M at the anode. In contrast, sulfuric acid-doped polybenzimidazole (s-PBI) membranes represent an alternative to membranes like Nafion because they do not rely on water for their proton conductivity. Figure 1 also shows the voltage and acid concentration for an SDE with sulfonated polybenzimidazole (s-PBI) operated at 110°C and 0.5 A/cm^2. Here we achieved 0.66 V with an acid concentration of 7.0 M. The acid concentration was varied by adjusting the water feed to the cell (i.e. water stoichiometry), which had little effect on the cell voltage. Consequently, these two performance metrics can be varied independently.

Therefore, polybenzimidazole (PBI) membranes offer the possibility of operating at high acid concentrations and/or elevated temperatures to minimize voltage losses (e.g., kinetic and ohmic resistances).[4,13–15] PBIs are a class of aromatic heterocyclic polymers that exhibit high thermal and chemical stabilities. PBI membranes have exceptional performance characteristics in various electrochemical devices due to their high ionic conductivity when imbibed with various acid electrolytes.[16–21] To date, a large variety of PBI polymers have been synthesized and studied, and a sulfonated polybenzimidazole was selected for use in SDE applications due to its stability in the sulfuric acid environments present in the electrolyzer,[13] which has resulted in an increased focus on PBI for SDE applications over the past several years.[19,22–24] These works focused on including different blends of PBI with high H_2SO_4 imbibed concentrations (80 wt%)[19,24] during membrane preparation, partially fluorinated PBI,[22,24] and crosslinked PBI.[23] However, these SDEs were operated with liquid water in the cathode, relying on water crossover to provide the water for Reaction 2 at the anode. No attempt was made to decouple the cell voltage and acid concentration produced in the anode.

Here, we analyze the voltage losses and acid concentration from an SDE operated using s-PBI membranes under a range of operating conditions. Namely, the current density was varied from 0.1 to 1.2 A/cm^2, the temperature from 80 to 122°C, and the water stoichiometry from 4 to 18. From the voltage data, kinetic parameters and membrane conductivity were obtained to better understand and quantify the individual potential contributions to the cell voltage. The measured acid concentrations were also compared to predictions from water balances coupled to a non-ideal vapor-liquid equation of state. The physical parameters obtained here enable the prediction of cell voltage and acid concentrations over a wide range of operating temperatures, pressures, currents and reactant flow rates.

Experimental

s-PBI was synthesized, as seen in Figure 2, with a pre-sulfonated monomer, mono-sodium-2-sulfoterephthalate, to ensure 100 percent sulfonation of the synthesized polymer.[21] The mono-sodium-2-sulfoterephthalate was combined with 3,3',4,4'-tetraaminobiphenyl in a 3-necked resin kettle equipped with nitrogen flow and an overhead mechanical stirrer. The solutions were heated to 195°C via a ramp and soak method, and allowed to sit at that temperature for 30–40 hours. The solutions were then held at 220°C for at least one hour before casting into films. The stir-rate and the temperature were monitored and controlled during the polymerization. Upon reaching an optimal casting viscosity, which was judged visually, the polymer solutions were poured onto a heated glass plate. Using a doctor's blade, the s-PBI solutions were drawn across the plates to a uniform thickness of 15 mils (381 microns). The glass plates containing the cast solution were immediately placed into a humidity controlled chamber at 55% ± 5% relative humidity (RH), 25°C ± 2°C. This method was used to drive the formation of gel membranes through the sol-gel process. Complete hydrolysis of the membranes occurred in under 24 hours. The final gel thickness was approximately 300–500 microns. The hydrolyzed polymer membranes with an area of at least 80 cm^2 directly cast from PPA solution were soaked in a de-ionized water bath for phosphoric acid removal, and the water bath pH was monitored to ensure complete phosphoric acid removal. The PBI membranes were then immersed in a 50 wt% H_2SO_4 bath for the imbibing procedure. After imbibing, titration analyses were conducted to verify that only sulfuric acid remained in the membrane. From this point, the membrane was visually inspected for uniformity and individual membranes were punched out for electrode fabrication.

The membrane was placed between two electrodes and hot-pressed at 140°C for 50–60 seconds using 2.0 × 10^{4}N (4500 lbs.) of force. The target compression for each MEA was 80% of its original thickness. The same electrode, obtained from BASF, was used on both the anode and cathode, and contained 1.0 mg/cm^2 platinum (Pt) catalyst loading.[21] The electrolyzer operation and acid-concentrations measurements are similar to previous works.[13] The exception is that water to humidify the SO_2 stream was directly injected into the feed stream at the entrance to the electrolyzer using a micropump rather than using a humidification bottle. The procedure enabled the water feed stream to be more accurately controlled, with no need for a pressure differential across the cell. For all data reported here, the catalyst loading was 1.0 mg Pt/cm^2 and SO_2 was fed in significant excess (5–10% single-pass conversion) to neglect concentration variations.

High frequency resistance (HFR) measurements were used to determine the membrane resistance for each MEA tested. Approximately 20 membranes were cut from two separate sheets and were tested and used to determine the trend in membrane resistance as a function of temperature, pressure, and current density.

When testing 10 cm^2 MEAs, the contents of the anode exit stream were collected in an airtight container pressurized and heated to the same conditions present in the electrolyzer to ensure that no water condensed out of the vapor phase and diluted the resulting acid. When collecting acid, the operating conditions were held constant for between 5 and 30 minutes until approximately 20 mL of liquid was obtained. A few membranes were held for much longer periods (~12 hr) in order to confirm that the acid concentration obtained from the 20 mL sample was representative of the operating conditions, as well as to ensure that water was accounted for, and not absorbing into or diffusing through the membrane.

Results and Discussion

The electrolyzer cell voltage is the sum of the equilibrium potential and the potential rises due to the ohmic resistance of the membrane, the cathodic overpotential, and the anodic overpotential as expressed in the following equation:

$$V = U_{eq} + iR_A + \eta_a + \eta_c \quad [5]$$

The cathodic overpotential in the electrolyzer, η_c, is due to kinetic losses in the production of hydrogen at the cathode. Due to the facile nature of this reaction on platinum, the cathodic overpotential was assumed to be negligible and set to zero for all conditions shown here.

Figure 3 shows the membrane resistance as a function of acid concentration. The data for Nafion was obtained from previous

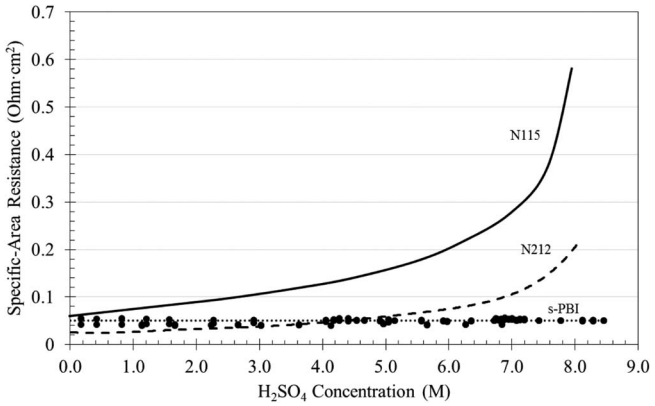

Figure 3. Specific area resistance as a function of sulfuric acid concentration for s-PBI obtained from multiple membranes compared to Nafion 115 and Nafion 212. $\Delta P = 600$ kPa for the Nafion membranes, and no pressure differential used for s-PBI.

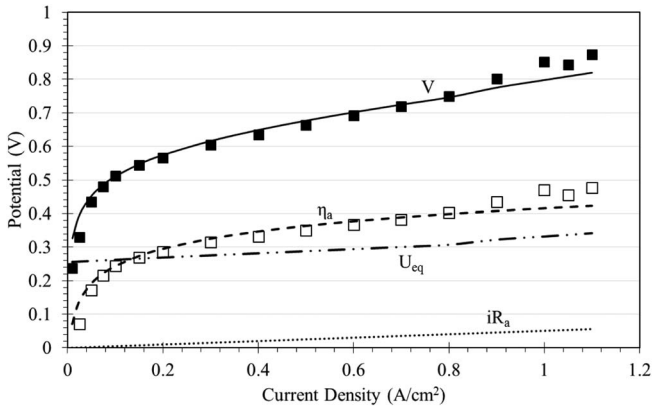

Figure 5. Individual potential contributions toward the overall cell voltage for the HyS electrolyzer at 110°C and a constant water feed rate of 0.45 mL/min. Lines represent model predictions and the symbols are the cell voltages (filled symbols) and anodic overpotentials (open symbols) data.

works.[8,11,12] The data for s-PBI were collected during 18 different tests on different membranes with the temperature ranging from 70°C to 125°C. As seen here, as the acid concentration produced in the SDE with a Nafion membrane is increased, the specific area resistance increases due to a decrease in the water content in the Nafion membrane.[8,9,11,12] However, an increase in acid concentration at the anode in the SDE operated with s-PBI shows no adverse effect on membrane resistance because the conductivity of s-PBI is not dependent on water to facilitate proton conduction. In addition, the measured resistance was not a function of temperature between 70°C to 125°C. Hence the average specific area resistance, R_A, for s-PBI across all temperatures and acid concentrations tested is 0.050 Ohm · cm^2, obtained via HFR measurements, and shown as the dotted line in Fig. 3. Therefore, even though a fully humidified Nafion 212 membrane is less resistive than s-PBI, these membranes outperform Nafion at high acid concentrations.

Figure 4 shows the sulfuric-acid concentration produced in the cell at 0.5 A/cm^2 and either 80°C or 110°C as a function of water stoichiometry. According to Eqn. 4, 2 moles of water are required for every mole of SO_2 consumed. Therefore, water stoichiometry refers to the ratio of the moles of water fed to the cathode to that required via Eqn. 4 at a given current. For example, 5 A are passed at 0.5 A/cm^2 for a 10 cm^2 MEA, which requires 51.8 μmol/s of water. Water stoichiometry of 10 means 518 μmol/s of water were fed. Increasing

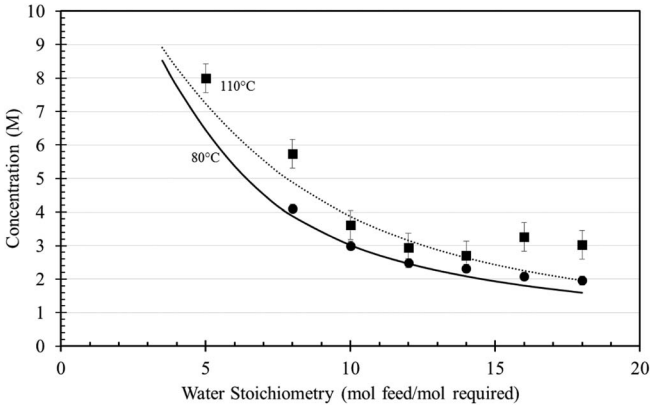

Figure 4. Sulfuric-acid concentrations produced in the cell at 0.5 A/cm^2 and either 80 (circles) or 110°C (squares) as a function of water stoichiometry. The water stoichiometry refers to the ratio of the moles of water fed to the cathode to that required via Eqn. 4 at a given current. The lines are the acid concentrations predicted from the Mixed Solvent Electrolyte Thermodynamics Framework (MSE) package in the OLI Systems, Inc. electrolyte software.

the water stoichiometry increases the excess of water and decreases the overall acid concentration in the exit stream. The symbols in Fig. 4 are the average of 1–3 data points for each stoichiometry at 80°C (12 data points total) and 2–4 data points for each stoichiometry at 110°C (24 data points total). Also shown in Fig. 4 are the model predictions generated from a water balance coupled to the Mixed Solvent Electrolyte Thermodynamics Framework (MSE) package in the OLI Systems, Inc. electrolyte software. The error bars represent the standard deviation of the difference between the experimental data and the model predictions (±0.1 and 0.4 M at 80°C and 110°C, respectively). The error bars are not visible at 80°C since they fall just within the symbols. The data collection was more reproducible at 80°C compared to 110°C because water condensation is easier to prevent at lower temperatures. In both cases though the trends show good agreement with the model predictions, confirming that the OLI electrolyte software can be used to accurately predict the sulfuric-acid concentration produced in the cell. In addition, accurate concentrations enables us to predict the equilibrium potential (U_{eq}) at different temperatures, pressures, currents, and reactant flow rates as described previously.[25]

Using the predicted values for U_{eq} from OLI and iR_A from the data in Fig. 3 (i.e., $R_A = 0.050$ Ohm · cm^2), the anodic overpotential was obtained from the measured cell voltage and Eqn. 5 at each temperature and current density (open symbols in Fig. 5). The kinetic parameters i_0 and α were obtained by fitting the anodic overpotential at currents ≤0.8 A/cm^2 to the following Tafel Expression at 80 and 110°C:

$$i = i_0 e^{\frac{2\alpha F \eta_a}{RT}} \quad [6]$$

The result was α = 0.22, which was assumed to be independent of temperature. This value of α was then used to fit the following Arrhenius relationship to the exchange current density obtained from the anodic overpotential data in Fig. 6 at 0.5 A/cm^2 and each temperature.

$$i_0 = i_{0,ref} e^{\frac{-E}{R}\left(\frac{1}{T} - \frac{1}{T_{ref}}\right)} \quad [7]$$

The result was $i_{0,ref}$ and E of $(4.1 \pm 0.07) \times 10^{-4}$ A/cm^2 and 116 ± 2 kJ/mol, respectively. T_{ref} is 353 K (80°C). Hence, Equations 6 and 7 can be used to predict the anodic overpotential at any temperature and current density.

Now that the individual voltage contributions can be predicted as a function of operating conditions, the individual potential contributions to the overall cell voltage can be examined. Again, Figure 5 shows the potential contributions to the cell voltage as a function of current density at 110°C and a constant water feed rate (variable water stoichiometry). The iR_A curve is linear because R_A was found to be constant at 0.05 Ohm · cm^2 (see Fig. 3). The anodic overpotentials

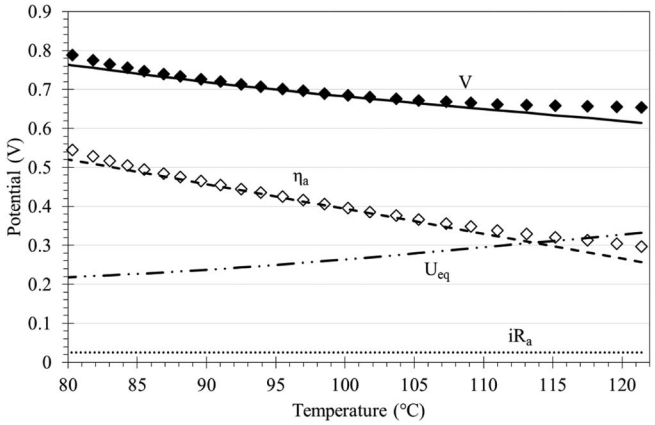

Figure 6. Contributions toward total operating voltage across a range of temperatures in the HyS electrolyzer at a current density of 0.5 A/cm^2 and a constant water flow rate of 0.50 mL/min. Lines represent model predictions and the symbols are the cell voltages (filled symbols) and anodic overpotentials (open symbols) data.

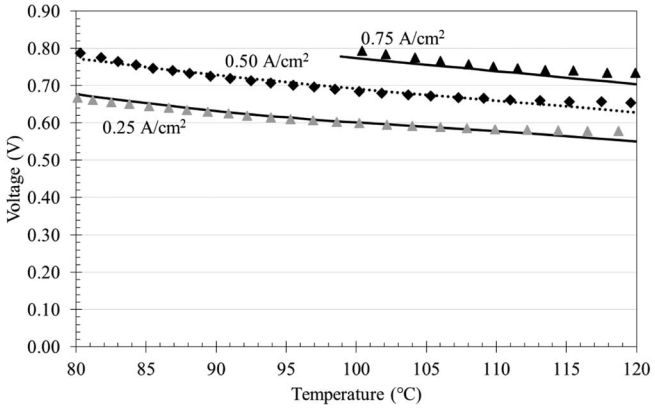

Figure 7. Model predictions compared to experimental data at three different current densities across a range of temperatures in the HyS electrolyzer at a constant water flow rate of 0.50 mL/min. The solid lines represent model predictions and dotted line represents the model fit at 0.5 A/cm^2 (i.e., same as the solid line in Fig. 6).

were predicted via Eqns. 6, and 7, and the equilibrium potentials were predicted using the OLI software in conjunction with thermodynamics examined in previous works.[25] At 0.5 A/cm^2, the cell voltage is approximately 660 mV, which consists of 290 mV from the equilibrium potential, 345 mV of anodic overpotential, and 25 mV iR_A drop due to membrane resistance. The largest contribution toward the total cell voltage at desired current densities is due to the anodic overpotential. From 0.2 to 1.0 A/cm^2, the cell voltage increases by 220 mV, with 150 mV of that coming from increased η_A. Although the membrane resistance increases with current, the small increase in iR_A is dwarfed by the increase in η_A and U_{eq}, the latter term associated with a slight increase in concentrations at higher currents due to a constant water feed for the data seen here.

Figure 6 shows the potential contributions to the cell voltage as a function of temperature at 0.5 A/cm^2 and a constant water stoichiometry. The cell voltage decreases from 730 mV at 90°C to 650 mV at 120°C. The equilibrium potential increases over that temperature range from 240 to 320 mV due to an increase in the acid concentration from 3.3 to 6 M, which follows the relationship observed previously.[25] However, this is more than offset by a decrease in η_A from 440 mV to 300 mV coupled with the benefit of iR_A being independent of acid concentration. The effect of water stoichiometry and system pressure on cell voltage was found to only occur through its effect on the equilibrium voltage via the acid concentration. That is, higher pressures (from 1 to 3 atm) or higher water stoichiometry (from 5 to 18) decreases the acid concentration and hence decreases the equilibrium voltage, but they do not measurably affect the membrane resistance or the anodic overpotential. Thus, the largest contribution to the overall cell potential is the anodic overpotential, which illustrates the area most deserving of future research. Figure 7 shows the model fit at 0.5 A/cm^2 and predictions at 0.25 A/cm^2 and 0.75 A/cm^2 compared to experimental data at three different current densities. Overall, there is good agreement between the model predictions and data between 0.25 A/cm^2 and 0.75 A/cm^2, which confirms the validity of the physical parameters obtained in this study.

Conclusions

The contributions of the equilibrium potential, anodic overpotential, and ohmic losses due to membrane resistance have been examined for the SDE operated with s-PBI membranes at elevated temperatures. The large anodic overpotentials that exists in this system suggest a need for improved catalysts, and that kinetics would improve with the higher temperatures afforded s-PBI membranes. Also, the specific-area resistance of the membrane was independent of temperature over the range of 70–120°C. In addition, the membrane resistance is not adversely affected by acid concentration, which offers benefits not seen when using Nafion. It was also seen that the pressure and water stoichiometry only affect the cell voltage via the equilibrium potential. All this should enable the voltage of an electrolyzer operated with s-PBI membranes to be reduced independently of high acid concentrations.

List of Symbols

E	Activation Energy, kJ/mol
F	Faraday's constant, 96485 C/mol
i	Current Density, A/cm^2
i_0	Exchange current density, A/cm^2
$i_{0,ref}$	Reference exchange current density, A/cm^2
R	Gas Constant, J/mol/K
R_A	Membrane Specific Area Resistance, Ohm · cm^2
T	Temperature, K
T_{ref}	Reference temperature, K
U_{eq}	Equilibrium potential, V
V	Cell Voltage, V

Greek

α	Transfer coefficient
η_a	Anodic Overpotential, V
η_c	Cathodic Overpotential, V

References

1. U.S.DRIVE, Hydrogen Production Technical Team Roadmap (2013).
2. Nuclear Hydrogen Research and Development Plan, *Department of Energy, Office of Nuclear Energy, Science and Technology* (2004).
3. C. Corgnale and W. A. Summers, *Int J Hydrogen Energ*, **36**, 11604 (2011).
4. J. W. Weidner, *J Appl Electrochem*, **46**, 829 (2016).
5. C. Corgnale, S. Shimpalee, M. B. Gorensek, P. Satjaritanun, J. W. Weidner, and W. A. Summers, *Int J Hydrogen Energ*, **42**, 20463 (2017).
6. M. B. Gorensek and W. A. Summers, *Int J Hydrogen Energ*, **34**, 4097 (2009).
7. P. W. T. Lu, E. R. Garcia, and R. L. Ammon, *J Appl Electrochem*, **11**, 347 (1981).
8. J. Staser, R. P. Ramasamy, P. Sivasubramanian, and J. W. Weidner, *Electrochem Solid St*, **10**, E17 (2007).
9. J. A. Staser, M. B. Gorensek, and J. W. Weidner, *J Electrochem Soc*, **157**, B952 (2010).
10. J. A. Staser, K. Norman, C. H. Fujimoto, M. A. Hickner, and J. W. Weidner, *J Electrochem Soc*, **156**, B842 (2009).
11. J. A. Staser and J. W. Weidner, *J Electrochem Soc*, **156**, B16 (2009).
12. J. A. Staser and J. W. Weidner, *J Electrochem Soc*, **156**, B836 (2009).
13. J. V. Jayakumar, A. Gulledge, J. A. Staser, C. H. Kim, B. C. Benicewicz, and J. W. Weidner, *Ecs Electrochem Lett*, **1**, F44 (2012).
14. T. R. Garrick, A. Gulledge, J. A. Staser, B. Benicewicz, and J. W. Weidner, *Ecs Transactions*, **61**, 11 (2014).
15. T. R. Garrick, A. Gulledge, J. A. Staser, B. Benicewicz, and J. W. Weidner, *Ecs Transactions*, **66**, 31 (2015).

16. K. J. Fishel, A. L. Gulledge, A. T. Pingitore, J. P. Hoffman, W. P. Steckle, and B. C. Benicewicz, *J Polym Sci Pol Chem*, **54**, 1795 (2016).
17. A. L. Gulledge, X. M. Chen, and B. C. Benicewicz, *J Polym Sci Pol Chem*, **52**, 619 (2014).
18. A. L. Gulledge, B. Gu, and B. C. Benicewicz, *J Polym Sci Pol Chem*, **50**, 306 (2012).
19. P. J. Cichon, A. J. Kruger, H. M. Krieg, D. Bessarabou, K. Aniol, and J. Kerres, *Int J Hydrogen Energ*, **41**, 4521 (2016).
20. L. Xiao, H. F. Zhang, E. Scanlon, L. S. Ramanathan, E. W. Choe, D. Rogers, T. Apple, and B. C. Benicewicz, *Chem Mater*, **17**, 5328 (2005).
21. J. A. Mader and B. C. Benicewicz, *Macromolecules*, **43**, 6706 (2010).
22. A. J. Kruger, P. Cichon, J. Kerres, D. Bessarabov, and H. M. Krieg, *Int J Hydrogen Energ*, **40**, 3122 (2015).
23. A. J. Kruger, J. Kerres, D. Bessarabov, and H. M. Krieg, *Int J Hydrogen Energ*, **40**, 8788 (2015).
24. H. Schoeman, H. M. Krieg, A. J. Kruger, A. Chromik, K. Krajinovic, and J. Kerres, *Int J Hydrogen Energ*, **37**, 603 (2012).
25. M. B. Gorensek, J. A. Staser, T. G. Stanford, and J. W. Weidner, *Int J Hydrogen Energ*, **34**, 6089 (2009).